ENVIRONMENTAL Science & Technology

ARTICLE

pubs.acs.org/est

Impedance Characteristics and Polarization Behavior of a Microbial Fuel Cell in Response to Short-Term Changes in Medium pH

Sokhee Jung,[†,∥] Matthew M. Mench,[‡,§] and John M. Regan*[,†]

[†]Department of Civil and Environmental Engineering,The Pennsylvania State University, University Park, Pennsylvania 16802, United States

[‡]Department of Mechanical, Aerospace, and Biomedical Engineering, University of Tennessee, Knoxville, Tennessee 37966, United States

[§]Energy and Transportation Science Division, Oak Ridge National Laboratory, Oak Ridge, Tennessee 37831, United States

ABSTRACT: pH oppositely influences anode and cathode performance in microbial fuel cells. The differential electrochemical effects at each electrode and the resultant full-cell performance were analyzed in medium pH from 6.0 to 8.0. Potentials changed −60 mV/pH for the anode and −68 mV/pH for the cathode, coincident with thermodynamic estimations. Open circuit voltage reached a maximum (741 mV) at pH 7, and maximum power density was highest (712 mW/m^2) at pH 6.5 as the cathode performance improved at lower pH. Maximum current density increased and apparent half-saturation potential (E_{KA}) decreased with increasing medium pH due to improved anode performance. An equivalent circuit model composed of two time constant processes accurately fit bioanode impedance data. One of these processes was consistently the rate-limiting step for acetate-oxidizing exoelectrogenesis, with its pH-varying charge transfer resistance R_2 ranging from 2- to 321-fold higher than the pH-independent charge transfer resistance R_1. The associated capacitance C_2 was 2−3 orders of magnitude larger than C_1. R_2 was lowest near E_{KA} and increased by several orders of magnitude at anode potentials above E_{KA}, while R_1 was nearly stable. However, fits deviated slightly at potentials above E_{KA} due to emerging impedance possibly associated with diffusion and excessive potential.

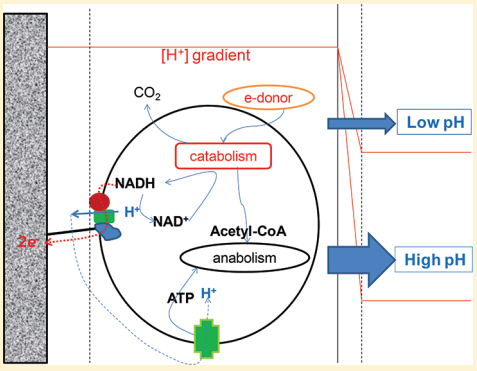

INTRODUCTION

Microbial fuel cells (MFCs) differ from electrochemical fuel cells in that they use microbes to catalyze reactions on the anode (and on the cathode in biocathode designs) instead of an inorganic catalyst. This requirement for maintaining a viable biocatalyst necessitates physiologically permissive medium conditions. An improved understanding of the catalytic activity of the bioanode as a function of solution conditions would contribute to enhanced MFC operation and performance. However, the electrochemistry of the bioanode is complex due to changing microbial communities and interactions within these communities in the anode biofilm.[1]

Electrochemical impedance spectroscopy (EIS) coupled with equivalent circuit (EC) analysis[2−4] has been used to elucidate anodic electrochemical reactions in MFCs. Development of anode biofilms significantly decreased anodic polarization resistance (interchangeable with charge transfer resistance), indicating their catalytic role in electron transfer to the anode.[5−8] In a ferricyanide-cathode MFC, initial development of anode biofilm during the first five days decreased anodic polarization resistance by ∼40% (from 2.6 to 1.5 kΩ cm^2 at 0.27 A/m^2) with a simultaneous increase in power density by ca. 120%.[7] In an air-cathode MFC, anodic charge transfer resistance decreased by ∼75% (from 0.073 to 0.017 kΩ cm^2 at 2.63 A/m^2) with increasing anodic capacitance during 70 days of long-term operation.[8]

To enable precise impedance analysis on extracellular electron transfer (exoelectrogenesis), pure cultures were also studied. Potentiostatic EIS on a *Geobacter sulfurreducens*-covered anode showed that charge transfer resistance was the lowest at the imposed potential near the midpoint potential in cyclic voltammetry.[6] In their impedance analysis, adding a second time constant through an additional circuit element did not improve data fitting.[6] In a subsequent study using *Shewanella oneidensis* DSP10, three RC time constants were used to differentiate three charge transfer reactions.[9]

One important controlling parameter for MFC performance is the medium pH. It was found that acidification of the anode biofilm affects current generation because microbial activity is inhibited in low pH.[10−12] For example, *G. sulfurreducens* grown using fumarate as an electron acceptor had a considerably lower growth rate at pH 6 (0.04 h^{-1}) than pH 7 (0.21 h^{-1}),[11] and riboflavin production by *S. oneidensis* DSP10 was reduced significantly at pH 5 with appreciably decreasing power compared with neutral pH.[13] It was demonstrated that alkaline medium and high buffer concentration enhances bioanode performance due

Received: May 22, 2011
Accepted: September 8, 2011
Revised: September 6, 2011
Published: September 08, 2011

to the increasing flux of proton shuttles out of the anode biofilm.[10,14] Increasing the pH from 7 to 9 resulted in a 42% improvement in maximum power density in a cloth-electrode assembly system.[14] Maximum current density at pH 8 was 9.9 A/m^2-anode, and only ca. 25% of this current was attained at pH 6 in a single-chamber microbial electrolysis cell (MEC).[10] Anode biofilm acidification was experimentally substantiated by fluorescent detection of the pH gradient in a pure *G. sulfurreducens* biofilm.[11] On the other hand, low pH enhances cathodic oxygen reduction, presumably due to increased availability of protons to participate in this reaction. It was observed that a lower pH created better performance in terms of current and power density in a granular-carbon cathode,[15] and it was also observed in an upflow MFC that lower catholyte pH benefitted cathodic oxygen reduction.[16] A 2.5-fold increase of maximum power density was observed with a catholyte of pH 1 compared to that of pH 7.5 in a two-chamber MFC.[17] Even in a biocathode, neutralizing the catholyte using strong acid was beneficial for current generation.[18]

We focused on characterizing the trade-off associated with differential performance effects of pH on each electrode, with acidic medium enhancing cathode performance but inhibiting bioanode performance. In varying pH conditions, impedance elements of the bioanode in a single-chamber MFC were characterized using a new equivalent circuit model. Furthermore, we characterized performance of each electrode and the whole cell using polarization behavior.

MATERIALS AND METHODS

MFC Construction and Operation. A single-chamber bottle MFC (350 mL) with a carbon paper anode (3.14 cm^2 projected area, E-TEK) and an air cathode (7 cm^2 of Pt-coated area, 0.5 mg Pt cm^{-2} Pt, and four PTFE diffusion layers) was constructed as previously described.[19,20] A Nylon membrane filter with 0.22 μm pores (Magna nylon, N02SP04700) was used to cover the solution-facing side of the cathode to prevent the formation of biofilm directly on the cathode. The small anode size and large medium volume allowed monitoring over long time periods without appreciable changes in the medium condition. A Ag/AgCl reference electrode was located 5 mm from the anode electrode. Anode biofilm enrichment was conducted in 50 mM phosphate-buffered GM medium (pH 7).[21] The MFC was inoculated with suspension from an electricity-producing MFC and operated with 10 mM sodium acetate (Sigma-Aldrich, MO) as an electron donor under 600 Ω of external resistance (R_{ext}) at 30 °C for 60 days for anode biofilm enrichment. Electrochemical tests were conducted upon observation of reproducible polarization behavior at a medium pH of 7. To characterize pH effects, GM media with pHs ranging from 6.0 to 8.0 at 0.5 pH unit increments were created with 5 M solutions of HCl or NaOH. The conductivities of these media were kept uniform at 8.9 mS/cm by adjusting with a 5 M solution of NaCl as needed.

Electrochemical Analysis. Before each electrochemical measurement, the MFC was operated for 4 h in the fresh medium condition, starting with a medium pH of 8.0 and decreasing incrementally to pH 6.0. Polarization tests, linear sweep voltammetry (LSV), and EIS were performed in separate batches for each pH condition. Between each pH change, the MFC was operated at the initial medium pH of 7 for 12 h. For all pH conditions, the final pH never decreased more than 0.2 pH units from the initial pH. After conducting each of these tests over the pH range, the entire operational procedure was repeated, and

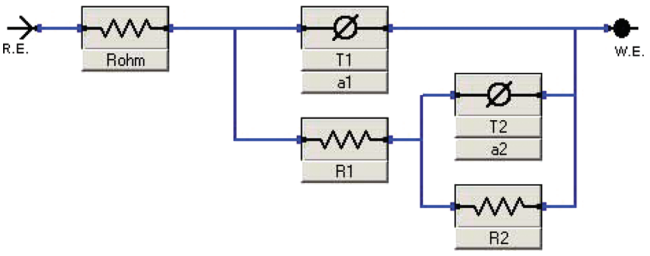

Figure 1. The proposed equivalent circuit, BIOANODE-1, models exoelectrogenic acetate oxidation occurring in the bioanode.

polarization tests were performed a second time at each pH. Averages and standard deviations of electrode potentials at each pH were calculated based on these replicated polarization tests. Polarization curves were created by decreasing R_{ext} from open circuit to 2 Ω and recording voltage after 30 min at each R_{ext} using a multimeter (Keithley Instruments, OH). LSV and EIS were performed using a potentiostat Reference 600 (Gamry Instrument Inc.). For LSV, the MFC circuit was disconnected for 2 h to create open circuit potential (OCP) for the anode. Then, a scan rate of 0.1 mV/s with a 1-mV step size was applied to the anode over the potential range from OCP to −0.2 V. For potentiostatic EIS, the bioanode was first either poised at each test potential until it produced stable current or disconnected for 2 h to attain OCP. Then EIS was performed at each DC potential with the following conditions: AC potential of 10 mV rms, initial frequency 10^6 Hz, final frequency 10 mHz, 10 points/decade of data acquisition.

Equivalent Circuit Model. Our BIOANODE-1 model (Figure 1) was composed of RC time constants representing two successive reactions of exoelectrogenic acetate oxidation. A constant phase element (CPE) was incorporated to model a nonideal capacitor, defined as $1/Z = T(j\omega)^{\alpha}$. T ($S \cdot s^{\alpha}$) is a numerical value of the admittance ($1/|Z|$) at $\omega = 1$, where S is siemens and s is second. The exponent α is an empirical nonideality constant, $j^2 = -1$, and ω (s^{-1}) is the radial frequency ($\omega = 2\pi f$).[22] Capacitance (C) is calculated using $C = (TR_p)^{1/\alpha}/R_p$, where R_p (Ω) is the charge transfer resistance.[22] Impedance spectra were fitted with the BIOANODE-1 model by χ^2-minimization using Echem Analyst (Gamry Instrument Inc.).

Calculations. The theoretical potentials of the anode and cathode in a specific medium condition were calculated using the Nernst equation according to eqs 1−4 for the tested pH range at 303 K (30 °C)

$$2HCO_3^- + 9H^+ + 8e^- \leftrightarrow CH_3COO^- + 4H_2O \quad (1)$$

$$E_{an,M} = E^o_{an} - \frac{RT}{8F}\ln\left(\frac{[CH_3COO^-]}{[HCO_3^-]^2[H^+]^9}\right), E^\circ = 0.187 \quad (2)$$

$$O_2 + 2H^+ + 2e^- \leftrightarrow H_2O_2 \quad (3)$$

$$E_{cat,M} = E^o_{cat} - \frac{RT}{2F}\ln\left(\frac{[H_2O_2]}{[O_2][H^+]^2}\right), E^\circ = 0.695 \quad (4)$$

E^o is the standard potential (at 298 K, 1 bar, 1 M, reported vs standard hydrogen electrode (SHE)), R is the ideal gas constant (8.314 J/Kmol), T is the temperature (K), and F is the Faraday constant (96,485C/mol-eq).[23] Potential values were reported

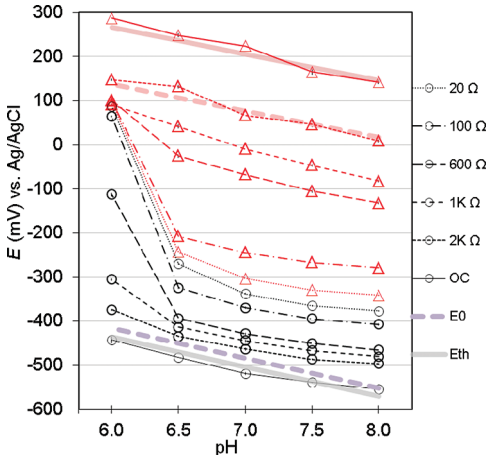

Figure 2. Averages and standard deviations of anode potential (E_{an}, circles) and cathode potential (E_{cat}, triangles) measured at different external resistances in medium pHs ranging from 6.0 to 8.0 (n = 2 based on replicated polarization tests across the entire pH range). Thick solid lines are theoretical potentials of the anode (bottom) and cathode (top) at approximate experimental conditions (cathode: $[H_2O_2]$ = 0.01 mM and $[O_2]$ = 0.2 atm, anode: $[CH_3COO^-]$ = 10 mM and $[HCO_3^-]$ = 5 mM, 303 K (30 °C)), and thick broken lines are standard potentials at 1 M or 1 atm of chemical species except for varying pH.

Table 1. Electrochemical Data in Each Medium pH from Polarization Curves[a]

pH	6.0	6.5	7.0	7.5	8.0
Anode OCP (mV)	−438	−482	−517	−539	−555
Cathode OCP (mV)	288	251	224	170	145
OCV (mV)	725	733	741	709	700
P_{max} (mW/m^2)	495	712	687	654	636
j_{max} (A/m^2)	1.85	4.69	5.01	5.05	6.15
E_{KA} (mV)	−352	−375	−416	−440	−431

[a] E_{KA} and j_{max} were calculated from LSV curves.

with respect to Ag/AgCl using Ag/AgCl = SHE − 197 mV.[24] Power density and current density were calculated using the apparent surface area of biofilm-covered anode (3.14 cm^2).

RESULTS

Polarization Behavior. Anode and cathode potentials were affected by the pH over the entire tested range of 6.0−8.0. As pH was lowered, both the anode potential (E_{an}) and the cathode potential (E_{cat}) increased (Figure 2 and Table 1), indicating that anode performance deteriorated and cathode performance was enhanced as bulk pH decreased. The OCP was described using the Nernst equation (Figure 2), assuming concentrations of 0.01 mM H_2O_2 at the cathode and 5 mM HCO_3^- and 10 mM acetate in the solution at the anode. These bicarbonate and acetate concentrations were the initial medium conditions, and this low hydrogen peroxide concentration provided the best fit to the cathode OCP data. Potential changes per pH unit increase were −60 mV/pH for the anode and −68 mV/pH for the cathode. Open circuit voltage (OCV) reached a maximum at pH 7, but maximum power density (P_{max}) was highest at pH 6.5 (Table 1). Maximum current density increased, and the midpoint potential

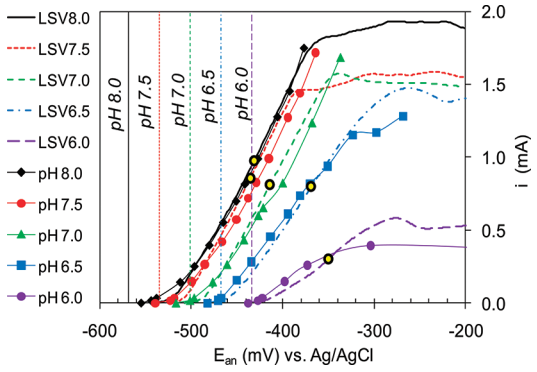

Figure 3. Linear sweep voltammetry (LSV, scan rate 0.1 mV/s) curves superimposed with anode polarization curves. Vertical lines are the theoretical open circuit potentials of the bioanode at a given pH calculated using the Nernst equation. Yellow circles designate midpoint potential (E_{KA}) values.

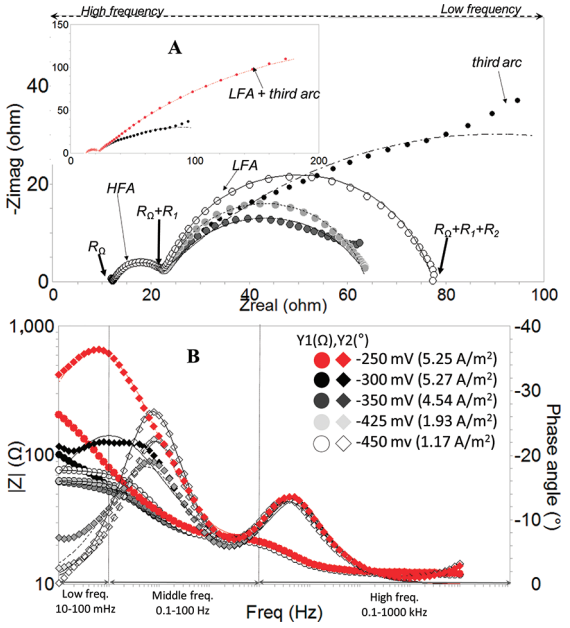

Figure 4. Bioanode impedance plots at E_{an} of −250, −300, −350, −425, and −450 mV in medium of pH 7. Points are experimental data, lines are fitted curves using the BIOANODE-1 equivalent circuit. A - Nyquist plot, B - bode plot.

(apparent half-saturation potential E_{KA} derived from LSV curves) decreased as pH increased (Table 1, Figure 3). At each medium pH, maximum current density was attained when E_{an} was approximately 100 mV greater than E_{KA}. Anode polarization curves superimposed on LSV curves illustrated that both methods yielded comparable results (Figure 3), except that an E_{an} range with a maximum current plateau was not observed using R_{ext} alterations (i.e., the polarization curve data) in high pH conditions. The duplicated polarization tests showed very high reproducibility of the reactor performance while subjected to the short-term pH perturbations.

Impedance Parameters of the Bioanode. The BIOANODE-1 model generated excellent fits to the impedance data (Figure 4). The χ^2 value ranged from approximately 10^{-4} to 10^{-3}.[25] Fits deviated slightly from experimental data above E_{KA}

dx.doi.org/10.1021/es201737g |Environ. Sci. Technol. 2011, 45, 9069–9074

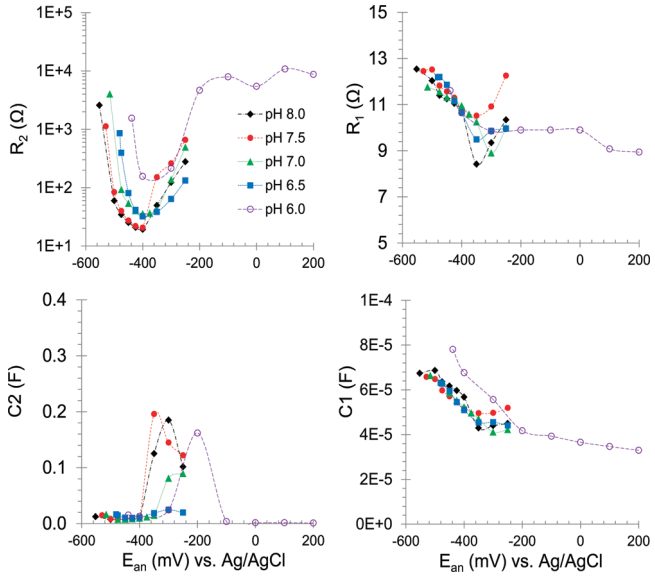

Figure 5. Parameter values from fittings of impedance data with the equivalent circuit BIOANODE-1. The lowest E_{an} for EIS was the OCP.

due to the emergence of a third arc at the lowest frequencies (Figure 4). The low frequency arc (LFA) and this third arc enlarged as E_{an} further increased above E_{KA}, and they finally combined into a single arc. However, χ^2 was still in the same order. Because the third impedance arc was not considered in the BIOANODE-1 model, impedance spectra at potentials below E_{KA} should be well-characterized using our model.

Medium pH did not affect R_1, but reducing medium pH increased R_2 (Figure 5). At potentials below E_{KA}, R_1 averaged $11.3 \pm 0.8\ \Omega$, and R_2 ranged from 2- to 321-fold higher than R_1. C_2 ($1.20 \times 10^{-2} \pm 0.47 \times 10^{-2}$ F) was 2 or 3 orders of magnitude larger than C_1 ($5.89 \times 10^{-5} \pm 0.77 \times 10^{-5}$ F). The nonideality constants were 0.80 ± 0.03 for α_1 and 0.78 ± 0.08 for α_2. Below E_{KA}, C_2 increased and C_1 decreased with increasing E_{an}. pH and E_{an} did not affect ohmic resistance (R_Ω, $12.4 \pm 0.8\ \Omega$) because it is related to electrode resistance, medium conductivity, and proximity of the reference electrode to the working electrode, all of which were constant throughout these experiments.

The presence of the third arc significantly affected fitting as indicated by the C_2 surge at potentials above E_{KA} (Figure 5). The nonideality constant α_2 fluctuated with E_{an} variations, but α_1 did not. Over the entire potential range, α_1 averaged 0.82 ± 0.04 and α_2 was 0.73 ± 0.12. In the overall potential range, R_2 ($1201.8 \pm 2552.4\ \Omega$) was 2 orders of magnitude greater than R_1 ($10.8 \pm 1.1\ \Omega$) (Figure 5). R_2 was lowest near the E_{KA} and increased 2 or 3 orders of magnitude above E_{KA}, while R_1 decreased by only a few ohms as E_{an} approached E_{KA} (Figure 5). Though impedance parameters generated from current-producing potentials had a consistent trend, those at OCP showed neither any consistency with the medium pH changes nor any correlation with the values attained from current-generating potentials (Table 1).

An abiotic control anode had an OCP of 510 mV at pH 7, which is close to the thermodynamic estimate for water hydrolysis. Acetate addition did not affect anode polarization, demonstrating that acetate was not oxidized abiotically at the anode. The Nyquist plot of the abiotic anode (not shown) consisted of two arcs. Impedance parameters of the abiotic anode at open circuit and pH 7 were $13.5\ \Omega$ for R_1, 4.3×10^{-5} F for C_1, 0.88 for α_1, $8.0 \times 10^7\ \Omega$ for R_2, 6.0×10^{-4} F for C_2, and 0.99 for α_2. R_1 and C_1 in the abiotic anode were slightly higher than the bioanode, but R_2 was 4 orders of magnitude larger and C_2 was 2 orders of magnitude larger.

DISCUSSION

Sequential reactions of microbial substrate oxidation and electron transfer via riboflavin were modeled in a previous equivalent circuit (EC) with three time constants.[9] However, this EC did not generate accurate fitting to our data. An EC for hydrogen oxidation in the anode of a PEM fuel cell [26] was used in this experiment. It consists of two processes, the electrosorption of hydrogen ($H_2 \leftrightarrow 2H_a$) and the electron transfer from hydrogen onto the anode interface ($H_a \leftrightarrow H^+ + e^-$).[26] While this EC provided an excellent fit to our EIS data, a complete mechanistic interpretation of these data from our MFC is precluded by factors such as the uncharacterized complexity of the microbial community, the associated mechanisms of charge transfer, the spatial heterogeneity of the biofilm, and the potential pH effects on all of these components. Increasing E_{an} lowered both the high- and low-frequency impedance in this study, showing that increasing E_{an} facilitated the overall kinetics of exoelectrogenic electron transfer to the solid anode surface at potentials below E_{KA}. However, current did not proportionally increase with increasing E_{an} above E_{KA}. R_1 and R_2 started to increase with increasing E_{an} above E_{KA}. While R_1 increased a slight amount, R_2 significantly increased due to the emergence of the third arc. Either proton diffusion resistance or excessive potential might increase those resistances.

The pH gradient between the anode biofilm and the medium controls the diffusion of protonated buffer species out of the biofilm, so that low medium pH limits current density.[10] Our results showed that R_2 was greatly affected by pH, while R_1 was insensitive to pH change (Figure 5). While microbial processes are generally sensitive to pH, it cannot be determined without additional targeted experiments which charge transfer reaction was captured by R_1 and insensitive to pH over the range of this study.

Diffusion of protonated species from the anode biofilm may be related to the third arc detected in the low frequency domain (Figure 4). Protons are produced during microbial substrate oxidation, which combine with buffer species such as carbonate or phosphate. Proton diffusion can be modeled by a Warburg element in equivalent circuits, usually shown as a straight line in the low frequency domain of a Nyquist plot. Pure diffusion creates a 45° line, but other factors such as capacitance influence the angle and curvature of the Warburg element. For example, mass transport processes for a porous gas diffusion electrode usually give a semicircle rather than a straight line in a Nyquist arc due to finite diffusion. [15,27] In PEM fuel cell systems, the main contributor to the overall impedance in low overpotential is normally charge transfer resistance (R_p), which is dependent on potential according to the Tafel equation $V \sim \log R_p^{-1}$, but diffusion resistance (mass transport resistance) becomes dominant in the overall impedance in high overpotential.[15] In our data, the third arc became a significant portion of total impedance at high current density in the saturating E_{an} region, appearing at potentials above E_{KA} and finally combining with the LFA, creating a semicircle (Figure 4). A two-chamber MFC did not have such an increase of impedance because of its low maximum current density (ca. 0.3 A/m^2-anode).[7,21] In a previous study, the lowest

charge transfer resistance (0.408 kΩ cm^2) was measured at an applied potential near the E_{KA} of −355 mV (−158 mV vs SHE) for *G. sulfurreducens*.[6] Our results also demonstrate charge transfer resistance was lowest near E_{KA} at each pH condition. We showed that medium pH affected E_{KA}, which has been regarded as an intrinsic constant of an anode biofilm.[28] These results imply that proton diffusion affects E_{KA}.

Charge transfer resistance R_1 (average ∼10 Ω) was minor compared with R_2 (average ∼400 Ω). At the maximum current density of our anode biofilm (6.8 A/m^2), the processes described by R_1 created ∼20 mV of potential loss, while the R_2 processes imposed ∼260 mV of potential loss (3.14 cm^2 of anode area × 6.8 A/m^2 × impedance Ω at 6.8 A/m^2). Future research should focus on discriminating the processes contributing to these discrete EIS signatures and engineering the exoelectrogenic microbial processes to minimize these overpotentials.

C_2 was several orders of magnitude greater than C_1, demonstrating higher charge storage in the LFA process(es) than the HFA process(es). The CPE is attributed to heterogeneous electrode properties or reactions (e.g., surface roughness, nonhomogeneous reaction rates on a surface, or variation of catalyst thickness).[29] The LFA had a higher α (0.82) than that of the HFA (0.73), but it is unknown whether this difference in nonideality is significant. C_2 increased sharply at anode potentials just above E_{KA}. In these potential ranges, EC fitting was not good due to the emergence of the third arc. So, this increase in the fitted C_2 value might be due to overestimation.

Anode performance was enhanced as the bulk pH was increased as previously shown.[30] This result was not consistent with a previous study using open circuit EIS, which showed the bioanode process preferred a neutral pH and had a slightly higher charge transfer resistance above neutral conditions.[13] Perhaps open circuit EIS might not be a representative way to evaluate electrode impedance in MFCs but rather closed-circuit conditions should be used.[15] Because anode catalysts are living microorganisms, the unavailability of an electron acceptor at open circuit might create unrepresentative impedance values, and current production (microbial respiration) should be allowed to characterize living microbial catalysts. Even in hydrogen fuel cells, the impedance data at current-generating potentials were suggested to be more representative of overall electrode processes than that at OCV with an exception that EIS of a symmetrical gas-feeding can be measured only at OCV.[15]

Alkaline electrolyte fuel cells have less cathodic activation overpotential than PEM fuel cells with an acidic electrolyte system.[31] In an alkaline electrolyte system, hydroxide ($O_2 + 4e^- + 2H_2O \leftrightarrow 4OH^-$) generated at the cathode is utilized for the anodic hydrogen oxidation ($2H_2 + 4OH^- \leftrightarrow 4H_2O + 4e^-$), where protons are not involved in the electrochemical reaction.[31] In a previous MFC study, the charge transfer resistance of the cathode decreased in high pH condition,[13] suggesting that their system behaved like an alkaline electrolyte system. In our result, high proton availability in low electrolyte pH led to improved cathode performance, demonstrated by increasing cathodic potential. Our thermodynamic estimations suggested that protons instead of hydroxide are involved in electrochemical reactions in our MFC system.

Although an acidic medium is beneficial for cathodic oxygen reduction, it decreases anodic substrate oxidation. High anode surface area, buffer concentration, or medium pH can prevent the acidification of anode biofilm because diffusion of protonated species is proportional to diffusive surface area, concentration of diffusive species, or pH gradient. Acidotolerant exoelectrogens might be another solution to pH inhibition. A strain of *Acidiphilium* sp. was able to produce up to 3 A/m^2-anode at ca.390 mV in aerobic low-pH medium, which leads to a low ohmic resistance configuration due to shorter distance between anode and air-cathode and high cathode performance due to high proton concentration.[32]

The BIOANODE-1 model created a nice fit to the experimental data as indicated by χ^2, even in the presence of a third arc. Addition of a CPE component allows the arc to elongate and match data, even though the real physical process may not be understood.[22] In our results, the third arc was not discretely modeled but rather was fitted with the LFA charge transfer resistance. A Finite Warburg element was added to our model, but it did not generate a well-matched fitting (data not shown). For future study, the BIOANODE-1 model can be improved by considering diffusion resistance in a high-flux system or excessive electrical energy in EC modeling.

AUTHOR INFORMATION

Corresponding Author

*Phone: 814-865-9436. Fax: 814-863-7304. E-mail: jregan@engr.psu.edu.

Present Addresses

‖Current address: Sustainability Consulting Group, Samsung SDS, Seoul, South Korea, 135-918.

ACKNOWLEDGMENT

This research was supported by National Science Foundation Grant CBET-0834033. The authors appreciate Dr. Xin Wang (Assistant Professor in Environmental Engineering, Nankai University) for his comments on this experiment, Dr. Kyu Taek Cho (Presently of the Environmental Energy Technologies Division, Lawrence Berkeley National Laboratory) for his explanations on fuel cell systems, and Dr. Judodine Patterson (Alcoa Technical Center, PA) for her manuscript revision. We also thank Dr. Digby Macdonald (Distinguished Professor in Material Science and Engineering, Penn State University) for his comments.

REFERENCES

(1) Jung, S.; Regan, J. M. Influence of external resistance on electrogenesis, methanogenesis, and anode prokaryotic communities in microbial fuel cells. *Appl. Environ. Microbiol.* **2011**, *77* (2), 564–571.

(2) Ciureanu, M.; Wang, H. Electrochemical impedance study of electrode-membrane assemblies in PEM fuel cells: I. Electro-oxidation of H_2 and H_2/CO mixtures on Pt-based gas-diffusion electrodes. *J. Electrochem. Soc.* **1999**, *146* (11), 4031–4040.

(3) Kim, J.-D.; Park, Y.-I.; Kobayashi, K.; Nagai, M.; Kunimatsu, M. Characterization of CO tolerance of PEMFC by AC impedance spectroscopy. *Solid State Ionics* **2001**, *140* (3−4), 313–325.

(4) Wagner, N.; Gulzow, E. Change of electrochemical impedance spectra (EIS) with time during CO-poisoning of the Pt-anode in a membrane fuel cell. *J. Power Sources* **2004**, *127* (1−2), 341–347.

(5) He, Z.; Huang, Y. L.; Manohar, A. K.; Mansfeld, F. Effect of electrolyte pH on the rate of the anodic and cathodic reactions in an air-cathode microbial fuel cell. *Bioelectrochemistry* **2008**, *74* (1), 78–82.

(6) Marsili, E.; Rollefson, J. B.; Baron, D. B.; Hozalski, R. M.; Bond, D. R. Microbial biofilm voltammetry: Direct electrochemical characterization of catalytic electrode-attached biofilms. *Appl. Environ. Microbiol.* **2008**, *74* (23), 7329–7337.

(7) Ramasamy, R. P.; Ren, Z. Y.; Mench, M. M.; Regan, J. M. Impact of initial biofilm growth on the anode impedance of microbial fuel cells. *Biotechnol. Bioeng.* **2008**, *101* (1), 101–108.

(8) Borole, A. P.; Aaron, D.; Hamilton, C. Y.; Tsouris, C. Understanding long-term changes in microbial fuel cell performance using electrochemical impedance spectroscopy. *Environ. Sci. Technol.* **2010**, *44* (7), 2740–2745.

(9) Ramasamy, R. P.; Gadhamshetty, V.; Nadeau, L. J.; Johnson, G. R. Impedance spectroscopy as a tool for non-intrusive detection of extracellular mediators in microbial fuel cells. *Biotechnol. Bioeng.* **2009**, *104* (5), 882–891.

(10) Torres, C. I.; Kato Marcus, A.; Rittmann, B. E. Proton transport inside the biofilm limits electrical current generation by anode-respiring bacteria. *Biotechnol. Bioeng.* **2008**, *100* (5), 872–81.

(11) Franks, A. E.; Nevin, K. P.; Jia, H.; Izallalen, M.; Woodard, T. L.; Lovley, D. R. Novel strategy for three-dimensional real-time imaging of microbial fuel cell communities: Monitoring the inhibitory effects of proton accumulation within the anode biofilm. *Energy Environ. Sci.* **2009**, *2* (1), 113–119.

(12) Gil, G. C.; Chang, I. S.; Kim, B. H.; Kim, M.; Jang, J. K.; Park, H. S.; Kim, H. J. Operational parameters affecting the performance of a mediator-less microbial fuel cell. *Biosens. Bioelectron.* **2003**, *18* (4), 327–334.

(13) Biffinger, J. C.; Pietron, J.; Bretschger, O.; Nadeau, L. J.; Johnson, G. R.; Williams, C. C.; Nealson, K. H.; Ringeisen, B. R. The influence of acidity on microbial fuel cells containing *Shewanella oneidensis*. *Biosens. Bioelectron.* **2008**, *24* (4), 900–905.

(14) Fan, Y. Z.; Hu, H. Q.; Liu, H. Sustainable power generation in microbial fuel cells using bicarbonate buffer and proton transfer mechanisms. *Environ. Sci. Technol.* **2007**, *41* (23), 8154–8158.

(15) Freguia, S.; Rabaey, K.; Yuan, Z.; Keller, J. G. Non-catalyzed cathodic oxygen reduction at graphite granules in microbial fuel cells. *Electrochim. Acta* **2007**, *53* (2), 598–603.

(16) Zhang, F.; Jacobson, K. S.; Torres, P.; He, Z. Effects of anolyte recirculation rates and catholytes on electricity generation in a litre-scale upflow microbial fuel cell. *Energy Environ. Sci.* **2010**, *3*, 1347–1352.

(17) Erable, B.; Etcheverry, L.; Bergel, A. Increased power from a two-chamber microbial fuel cell with a low-pH air-cathode compartment. *Electrochem. Commun.* **2009**, *11* (3), 619–622.

(18) Liang, P.; Fan, M.; Cao, X.; Huang, X. Evaluation of applied cathode potential to enhance biocathode in microbial fuel cells. *J. Chem. Technol. Biotechnol.* **2009**, *84* (5), 794–799.

(19) Logan, B.; Cheng, S.; Watson, V.; Estadt, G. Graphite fiber brush anodes for increased power production in air-cathode microbial fuel cells. *Environ. Sci. Technol.* **2007**, *41* (9), 3341–3346.

(20) Cheng, S.; Liu, H.; Logan, B. E. Increased performance of single-chamber microbial fuel cells using an improved cathode structure. *Electrochem. Commun.* **2006**, *8* (3), 489–494.

(21) Jung, S.; Regan, J. M. Comparison of anode bacterial communities and performance in microbial fuel cells with different electron donors. *Appl. Microbiol. Biotechnol.* **2007**, *77* (2), 393–402.

(22) Macdonald, J. R. Impedance spectroscopy. *Ann Biomed. Eng.* **1992**, *20* (3), 289–305.

(23) Logan, B. E. *Microbial fuel cells*; Wiley-Interscience: 2008.

(24) Bard, A.; Faulkner, L. *Electrochemical methods: Fundamentals and applications*; John Wiley & Sons: 2001.

(25) Taylor, J. *An introduction to error analysis: The study of uncertainties in physical measurements*; Univ Science Books: 1997.

(26) Ciureanu, M.; Mikhailenko, S. D.; Kaliaguine, S. PEM fuel cells as membrane reactors: Kinetic analysis by impedance spectroscopy. *Catal. Today* **2003**, *82* (1−4), 195–206.

(27) Xie, Z.; Holdcroft, S. Polarization-dependent mass transport parameters for ORR in perfluorosulfonic acid ionomer membranes: An EIS study using microelectrodes. *J. Electroanal. Chem.* **2004**, *568*, 247–260.

(28) Marcus, A. K.; Torres, C. I.; Rittmann, B. E. Conduction-based modeling of the biofilm anode of a microbial fuel cell. *Biotechnol. Bioeng.* **2007**, *98* (6), 1171–1182.

(29) Baron, D. B.; Labelle, E.; Coursolle, D.; Gralnick, J. A.; Bond, D. R. Electrochemical measurement of electron transfer kinetics by *Shewanella oneidensis* MR-1. *J. Biol. Chem.* **2009**, *284* (42), 28865–28873.

(30) Yuan, Y.; Zhao, B.; Zhou, S.; Zhong, S.; Zhuang, L. Electrocatalytic activity of anodic biofilm responses to pH changes in microbial fuel cells. *Bioresour. Technol.* **2011**, *102* (13), 6887–91.

(31) Mench, M. M. *Fuel cell engines*; John Wiley and Sons, Inc.: New York, NY, 2008.

(32) Malki, M.; De Lacey, A. L.; Rodriguez, N.; Amils, R.; Fernandez, V. M. Preferential use of an anode as an electron acceptor by an acidophilic bacterium in the presence of oxygen. *Appl. Environ. Microbiol.* **2008**, *74* (14), 4472–6.